Multigrid approach in shifted linear systems for the non-degenerated twisted mass operator

Constantia Alexandrou[a,b], Simone Bacchio[a,c], Jacob Finkenrath[b]

[a]Department of Physics, University of Cyprus, PO Box 20537, 1678 Nicosia, Cyprus

[b]Computation-based Science and Technology Research Center, The Cyprus Institute

[c]Fakultät für Mathematik und Naturwissenschaften, Bergische Universität Wuppertal

Abstract

Application of multigrid solvers in shifted linear systems is studied. We focus on accelerating the rational approximation needed for simulating single flavor operators. This is particularly useful, in the case of twisted mass fermions for mass non-degenerate quarks and can be employed to accelerate the $N_f = 1 + 1$ sector of $N_f = 2 + 1 + 1$ twisted mass fermion simulations. The multigrid solver is accelerated by employing suitable initial guesses. We propose a novel strategy for proposing initial guesses for shifted linear systems based on the Lagrangian interpolation of the previous solutions.

1 Introduction

Simulation of lattice Quantum Chromodynamics (QCD) is computationally very demanding due to the requirement of solving a large number of linear system equations, which involve very large sparse complex matrices. A specific kind of these linear equations of focus in this paper, is given by multi-shifted systems

$$(Q^2 + m_i^2 I) \, x_i = b \tag{1.1}$$

for a set of different shifts m_i acting on the diagonal of the squared operator Q and where all shifts depend on a common right hand side b. Speeding-up the time to solution is essential for performing the simulation and we discuss how this is achieved within a multigrid approach. Multigrid approaches can be efficient for the case that the operator Q develops very small eigenvalues, thus yielding iteration counts of $\mathcal{O}(1000)$ when using approaches based on non-preconditioned Krylov subspace methods.

Shifted linear systems, here referred to as multi-mass shifted systems, have to be solved if the square root of a matrix is evaluated via rational, polynomial approximations (see e.g. [1,2]) or by using an integral definition via Stieltjes function [3,4]. In general the matrix roots have to be calculated in case of Monte Carlo simulations involving a single quark [2]. Another application of the matrix square root is given by the calculation of the Neuberger overlap operator [5].

The approaches routinely used to solve shifted linear equations like Eq. (1.1) are given by Krylov space solvers [3,4,6–8]. In what follows we will refer to the multi-mass shift conjugated gradient (MMS-CG) solver as the "standard" solver [6,7]. The advantage of multi-mass

shifts solvers is that the numerical effort scales only with the cost for solving the smallest shift and thus is almost independent of the total number of shifts. The idea behind these approaches is to exploit the identical eigenspaces by using the same Krylov space generated for the most ill-conditioned system to iterate all other shifts. However, if the operator Q^2 develops very small eigenvalues, flexible preconditioned iterative solvers can be by far more effective as compared to the conjugate gradient solver.

The central idea of this paper is to introduce a hybrid method, using MMS-CG solver for systems with a larger mass-shift, while for the systems with the smaller shifts employ a multi-grid approach using extrapolated initial guesses. The novelty of this method is how these initial guesses are constructed. We will discuss two approaches, one using Lagrange interpolation based on the solution of other shifts and the second using the MMS-CG solver to construct guesses which will be used for the systems involving the smallest mass-shifts.

For very ill-conditioned systems a very effective approach is given by multigrid methods as a preconditioner for Krylov solvers [9–11]. Multigrid solvers optimized for lattice QCD fermion operators show a very good scaling down to the physical light quark mass and can speed-up the time to solution by more than two order of magnitude compared to standard Krylov methods like the conjugate gradient (CG) solver. The idea is to use a coarse grid correction to tackle small eigenvalues and a smoother to tackle large eigenvalues in each iteration. However, all multigrid approaches are optimized to solve a linear equation where only a single operator is involved, as given by $Qx = b$. This will not hinder the solution of the squared systems but introduces different ways to tackle the multi-mass shifted system of Eq. (1.1) given by two consecutive solves of the single systems or taken the difference of two solve of the single system. Moreover, given the fact that state-of-the-art simulations are being performed using increasingly larger lattice sizes, a closer look to the different ways by discussing the involved stopping criteria seems advisable.

Multigrid approaches in lattice QCD are known for a variety of fermion discretizations, such as for the Wilson fermion discretization [9–11], as a preconditioner for Neuberger overlap fermions [12], for Domain Wall fermions [13] or for staggered fermions [14]. In this work we consider twisted mass fermions [15] and extend the approach of Ref. [16] for the more general case of using a doublet of twisted mass fermions with different masses. As in Ref. [16], we adapt the adaptive aggregation-based domain decomposition multigrid (DD-αAMG) approach and show how the symmetries of the non-degenerated twisted mass operator can be successfully used to build a coarse grid correction.

The paper is organized as follows: In section 2 we discuss how the fermion operator, here represented by Q, can be constructed on a four dimensional lattice, giving in detail the representation of a doublet of twisted mass fermions with different masses. In section 3 we explain the DD-αAMG approach and how it can be used to solve a linear equation that involves a squared operator $Q^2x = b$, especially when large lattice sizes are used and in the presence of small quark masses. We then present how the DD-αAMG approach can be adapted to the non-degenerated (ND) twisted mass operator. This involves a discussion of the properties of the ND twisted mass operator and how this can be used to construct a coarse grid corrections. At the end of the section we show numerical results. In section 4 we present the central idea of this work, namely the solution of the multi-mass shifted systems via a hybrid approach. For that we first introduce the approximation used for the square root matrix function, given by a rational approximation and explain how to construct initial guesses via Lagrange interpolation and from the MMS-CG solver. To illustrate the effectiveness of our approach we present results

using $N_f = 2 + 1 + 1$ gauge-configurations at physical quark masses.

2 Wilson twisted mass fermions

Solving Eq. (1.1), requires the inverse of a very large sparse matrix, which depends on the discretization scheme of the fermionic action. We consider here the two flavor non-degenerated twisted mass operator given by [15]

$$
D_{\mathrm{ND}}(\bar{\mu}, \bar{\epsilon}) = (D_{\mathrm{W}} \otimes I_2) + i\bar{\mu}\left(\Gamma_5 \otimes \tau_3\right) - \bar{\epsilon}(I \otimes \tau_1) = \begin{bmatrix} D_{\mathrm{W}} + i\bar{\mu}\Gamma_5 & -\bar{\epsilon}I \\ -\bar{\epsilon}I & D_{\mathrm{W}} - i\bar{\mu}\Gamma_5 \end{bmatrix}
$$
$$
= \begin{bmatrix} D_{\mathrm{TM}}(\bar{\mu}) & -\bar{\epsilon}I \\ -\bar{\epsilon}I & D_{\mathrm{TM}}(-\bar{\mu}) \end{bmatrix} \tag{2.1}
$$

with the bare mass parameters $\bar{\mu}$ and $\bar{\epsilon} \in \mathbb{R}$. The twisted mass terms $\bar{\mu}$ and $\bar{\epsilon}$ act on the two-dimensional flavor space and τ are the Pauli matrices.

$$
\tau_1 = \begin{pmatrix} & 1 \\ 1 & \end{pmatrix} \quad \text{and} \quad \tau_3 = \begin{pmatrix} 1 & \\ & -1 \end{pmatrix}. \tag{2.2}
$$

The twisted mass (TM) Wilson Dirac operator

$$
D_{\mathrm{TM}}(\mu) = D_{\mathrm{W}} + i\mu\Gamma_5 \tag{2.3}
$$

acts on the single flavor space $\mathcal{V}_s = \mathcal{V} \times \mathcal{S} \times \mathcal{C}$ with $\mathcal{S}$ the spin space and $\mathcal{C}$ the color space. The spatial volume $\mathcal{V} = T \cdot L^3$ is the four-dimension hyper-cubic lattice defined by

$$
\mathcal{V} = \{x = (x_0, x_1, x_2, x_3), 1 \le x_0 \le T, \ 1 \le x_1, x_2, x_3 \le L\} \tag{2.4}
$$

with T the number of points in the temporal direction and L the number of points in the spatial directions x, y and z. The matrix $\Gamma_5 = I_\mathcal{V} \otimes \gamma_5 \otimes I_\mathcal{C}$ is based on the spin space component γ_5, which can be represented by $\gamma_5 = \gamma_0\gamma_1\gamma_2\gamma_3 = diag\{ \ 1, \ 1, -1, -1\}$ in the so-called chiral representation. Note that we set the lattice spacing a to unity throughout this paper. The TM Wilson operator is itself based on the Wilson Dirac operator $D_{\mathrm{W}} \equiv D_{\mathrm{W}}(U, m, c_{sw})$ given by

$$
(D_{\mathrm{W}}\psi)(x) = \Big((m+4)I_{12} - \frac{c_{sw}}{32} \sum_{\mu,\nu=0}^{3} (\gamma_\mu\gamma_\nu) \otimes \big(Q_{\mu\nu}(x) - Q_{\nu\mu}(x)\big)\Big)\psi(x)
$$
$$
- \frac{1}{2}\sum_{\mu=0}^{3} \left((I_4 - \gamma_\mu) \otimes U_\mu(x)\right)\psi(x + \hat{\mu})
$$
$$
- \frac{1}{2}\sum_{\mu=0}^{3} \left((I_4 + \gamma_\mu) \otimes U_\mu^\dagger(x - \hat{\mu})\right)\psi(x - \hat{\mu}), \tag{2.5}
$$

with m the mass parameter and c_{sw} the parameter of the clover term [17], for a definition of $Q_{\nu\mu}(x)$ see e.g. Ref. [16]. The gauge links $U_\mu(x)$ are $SU(3)$ matrices, and the set $\{U_\mu(x) : x \in \mathcal{L}, \ \mu = 0, 1, 2, 3\}$ is referred to as a gauge configuration. The γ-matrices act on the spin degrees of freedom of the spinor field $\psi(x)$ and fulfill the anti-commutation relation $\{\gamma_\mu, \gamma_\nu\} = 2 \cdot I_4 \, \delta_{\mu\nu}$.

3

Often the Wilson Dirac operator is decomposed using an even-odd reduction. This is possible because the operator couples only next neighboring points. Even-odd reduction has several advantages compare to the full operator: it reduces the dimension of the operator and increases effectively the smallest eigenvalue by a factor two (see e.g. [16]). Even-odd reduction is commonly used in lattice QCD and in what follows we will use it throughout for the ND twisted mass operator. This yields an overall speed up for the time to solution in the case of the CG solver by a factor two. However, if a multigrid solver is used the linear equation system with the full operator is solved because the complexity of the structure increases in case of the even-odd reduced operator due to next-to-next neighbor interaction. For more details we refer to Ref. [16].

In this paper, we consider the ND twisted mass operator for $\bar{\epsilon} > 0$. Due to the flavor mixing, introduced by the off-diagonal term proportional to $\bar{\epsilon}$, the renormalized quark masses for the strange and charm doublet, m_s and m_c respectively, are connected to the bare twisted mass parameters by

$$m_s = \frac{1}{Z_P}\mu_s = \frac{1}{Z_P}\bar{\mu} - \frac{1}{Z_S}\bar{\epsilon} \qquad \text{and} \qquad m_c = \frac{1}{Z_P}\mu_c = \frac{1}{Z_P}\bar{\mu} + \frac{1}{Z_S}\bar{\epsilon} \qquad (2.6)$$

where Z_S is the scalar and Z_P is the pseudoscalar renormalization constants. For $\bar{\epsilon} = 0$ the masses are degenerated, as currently employed in the simulations for the light quark sector with a mass-degenerated quark doublet representing the up- and down-quark. The twisted mass discretization is free of $\mathcal{O}(a)$ effects if the light quark sector is tuned to maximal twist [18, 19]. This is achieved by tuning the Partially Conserved Axial Current (PCAC) mass, m_{PCAC}, to zero, i.e by demanding that $m_{\text{PCAC}} \to 0$.

The ND twisted mass operator is $(\Gamma_5 \otimes \tau_1)$-hermitian:

$$Q_{\text{ND}}(\bar{\mu}, \bar{\epsilon}) = (\Gamma_5 \otimes \tau_1)\, D_{\text{ND}}(\bar{\mu}, \bar{\epsilon}) = D_{\text{ND}}^{\dagger}(\bar{\mu}, \bar{\epsilon})\,(\Gamma_5 \otimes \tau_1) = Q_{\text{ND}}^{\dagger}(\bar{\mu}, \bar{\epsilon}). \qquad (2.7)$$

due to the Γ_5-hermiticity of the Wilson Dirac operator

$$Q_{\text{W}} = \Gamma_5 D_{\text{W}} = D_{\text{W}}^{\dagger}\Gamma_5 = Q_{\text{W}}^{\dagger}. \qquad (2.8)$$

For the determinant of the ND twisted mass operator, it follows that

$$\det\left[D_{\text{ND}}(\bar{\mu}, \bar{\epsilon})\right] \in \mathbb{R} \qquad (2.9)$$

using the $(\Gamma_5 \otimes \tau_1)$-hermiticity. This implies the positiveness of the determinant. The positiveness of the operator [18] is achieved for $\bar{\mu} > \bar{\epsilon}$. In case of the heavy quark doublet, for physical values of the strange and charm quark masses, this is achieved if the ratio of the renormalization constants is given by $Z_P/Z_S > 0.85$. However, numerically it is found that this bound is too strict, e.g. we found a gap for the smallest eigenvalue for the case of $Z_P/Z_S = 0.8$ as shown in Fig. 1. We measured the distribution of the smallest and largest eigenvalues of the squared even-odd reduced ND twisted mass operator on an ensemble of gauge configuration with a lattice volume of $V = 128 \times 64^3$ and a finite lattice spacing of $a \sim 0.08$ fm, discussed in detail in [20]. We will denote this ensemble as our physical test ensemble and it will be used throughout this paper to numerically validate our approach. It is generated with fermion parameters, such that the light, strange and charm quark masses are tuned close to their physical values, with $\mu = 0.00072$ being the light quark mass parameter and with $\bar{\mu} = 0.12469$ and $\bar{\epsilon} = 0.13151$ being the heavy quark bare mass parameters of the ND twisted mass operator. Moreover in the tests we employ the ND twisted mass operator also for the light quark sector using $\bar{\mu}_{\ell} = 0.00072$ and $\bar{\epsilon}_{\ell} = 0.000348$.
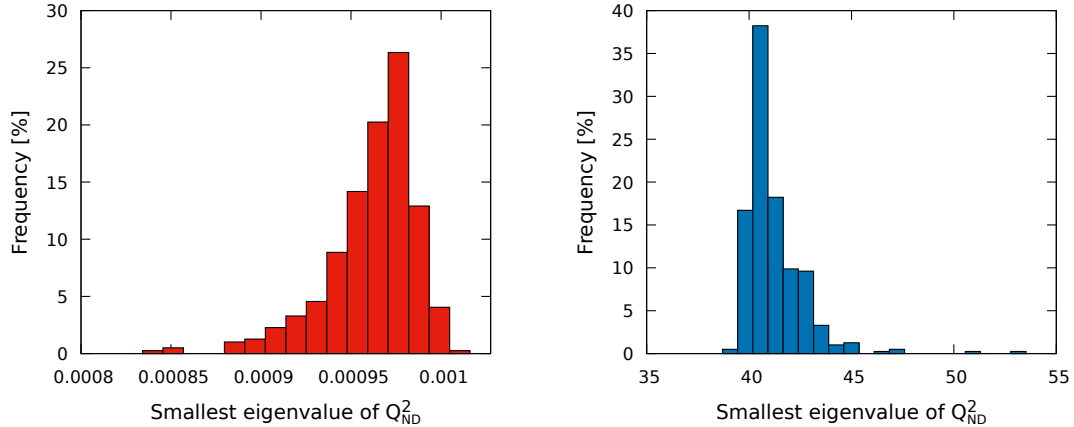
Figure 1: Distribution of the smallest (left) and largest (right) eigenvalues of the squared even-odd reduced ND twisted mass operator using an ensemble of gauge-configurations tuned to the physical values of the light, strange and charm quark masses.

3 DD-αAMG approach for twisted mass Wilson fermions

There exist several multigrid approaches for the Wilson Dirac operator [9–11]. In this section, we outline the adaptive aggregation-based domain decomposition multigrid (DD-αAMG) method for the Wilson Dirac operator [11] and TM operator [16]. The method is based on a flexible iterative Krylov solver, which is preconditioned at every iteration step by a multigrid approach. The preconditioner acts on the error propagation through

$$\epsilon \leftarrow \left(I - MD_{\mathrm{W}}\right)^k \left(I - PD_{\mathrm{W},c}^{-1}P^\dagger D_{\mathrm{W}}\right) \left(I - MD_{\mathrm{W}}\right)^j \epsilon, \tag{3.1}$$

where the coarse grid correction $PD_{\mathrm{W},c}^{-1}P^\dagger$ is applied with k pre- and j post-iteration of the smoother M. The multigrid preconditioner exploits domain decomposition strategies: the smoother M is given by the Schwarz Alternating Procedure (SAP) [21] and the coarse grid operator $D_{\mathrm{W},c} = P^\dagger D_{\mathrm{W}}P$ is based on an aggregation-based projection with the prolongation operator P. The method is designed to deal efficiently with both, infrared (IR) and ultra-violet (UV) modes of the operator D_{W}. The smoother reduces the error components belonging to the UV-modes [11], while the coarse grid correction is designed to deal with the IR-modes. This is achieved by using an interpolation operator P, which approximately spans the eigenspace of the small eigenvalues. Thanks to the property of local coherence [9], the subspace can be approximated by aggregating over a small set of $N_v \simeq \mathcal{O}(20)$ test vectors v_i, which are computed in the DD-αAMG method via an adaptive setup phase [11]. We remark that the prolongation operator is Γ_5-compatible, i.e. $\Gamma_5 P = P\Gamma_{5,c}$. This guarantees the Γ_5-hermiticity of the coarse grid operator D_c, i.e. $D_c^\dagger = \Gamma_{5,c}D_c\Gamma_{5,c}$ with $\Gamma_{5,c} = I_{\mathcal{V}_c} \otimes \sigma_3 \otimes I_{N_v}$ being the coarse grid equivalent of Γ_5. On the coarsest grid, even-odd reduction is used to accelerate the time solution.

The DD-αAMG approach has been adapted to the TM Wilson operator $D_{\mathrm{TM}}(\pm\mu)$ by modifying the coarse grid procedure in order to avoid the slowing down of the time to solution for small $\mu \ll 1$ by the coarse grid correction step. This is circumvent by effectively reducing the iterations for the coarse grid by using a larger μ for the coarse operator. i.e. $D_{\mathrm{TM},c}(\pm d\mu) = D_{\mathrm{W},c} \pm id\mu\Gamma_{5,c}$ with $d \geq 1$ [16]. For $d \sim 5$ the iterations count for inverting the coarsest operator
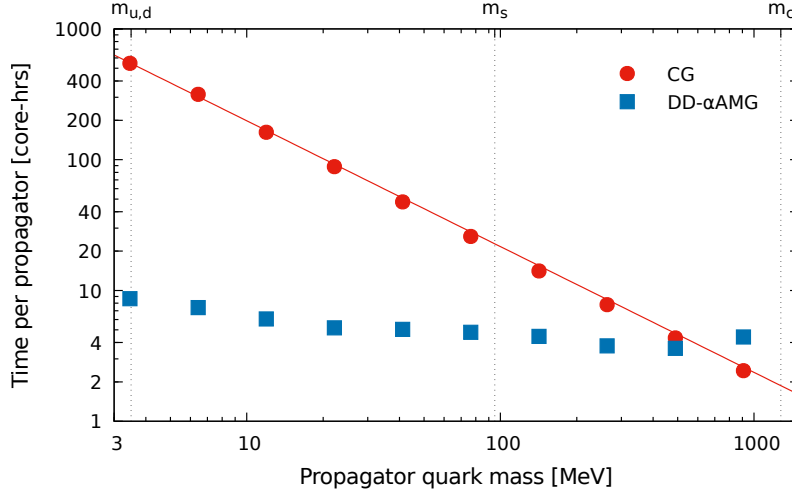
Figure 2: Comparison between time to solution for computing the twisted mass fermion propagator at different quark mass using the odd-even (oe) CG solver and the DD-αAMG approach. The results are for a 128×64^3 ensemble simulated at physical pion mass, $m_\pi \sim 135$ MeV. The value of the light, strange and charm quark masses are shown by the vertical lines with the labels $m_{u,d}$, m_s and m_c, respectively.

is reduced by an order of magnitude while it affects only marginally the outer solver iterations count. This yields a compatible speed-up for the time to solution when using the DD-αAMG approach for TM Wilson fermions as was obtained for the case of Wilson fermions [11].

3.1 Solving the squared linear equation

Before we introduce the new, adapted, multigrid approach for the ND twisted mass operator, we make some general remarks about solving a linear equation involving a squared Dirac operator. Solving the linear Dirac equation involving a hermitian operator is needed within lattice QCD in several places such as for the fermion force calculation during the Hybrid Monte Carlo (HMC) simulation or the calculation of matrix functions, like the square root or the sign function of the Dirac operator. Let us consider linear equations of the form

$$(Q_{\mathrm{W}}^2 + \mu^2)x = b \tag{3.2}$$

involving a squared operator Q_{W}^2, which in our case, is the square of the TM Wilson operator. We will denoted here the direct solution of eq. (3.2) as case **A**. A standard approach to solve such equation is to use the conjugate gradient (CG) solver. However, when one approaches the physical value of the light quark mass, the efficiency of the CG solver suffers due to the increase of the number of small eigenvalues. In this parameter range, multigrid approaches are by far more effective as shown in Fig. 2 for the case of the TM Wilson operator. However, the multigrid approach outlined in the previous section, can only be applied to a linear equation with a single TM Wilson operator. The reason is simply that an implementation for the squared operator is far more complicated, involving next to next neighbor interactions, which increase the complexity of the coarse operator. A way to solve Eq. (3.2) is to modify it by exploiting the Γ_5-hermiticity resulting into two sequential inversions, denoted here as case **B**,

$$(Q_{\mathrm{W}}^2 + \mu^2)^{-1}b = (Q_{\mathrm{W}} \pm i\mu)^{-1}(Q_{\mathrm{W}} \mp i\mu)^{-1}b \, . \tag{3.3}$$

6

Note that this can be done in a similar way for the ND operator using the $(\Gamma_5 \otimes \tau_1)$-hermiticity. However, splitting up Eq. (3.2) is not unique and another possibility is given by a difference of the two single inversions, denoted here as case **C**,

$$(Q_{\mathrm{W}}^2 + \mu^2)^{-1} b = \frac{i}{2\mu} \left((Q_{\mathrm{W}} + i\mu)^{-1} b - (Q_{\mathrm{W}} - i\mu)^{-1} b \right) . \tag{3.4}$$

In exact arithmetic all ways yield to the same solution. This is not so obvious anymore if iterative solvers are used since they involve a stopping criterium. A standard procedure is to stop the solver if the relative residual $\|r\| / \|b\|$ is smaller than a chosen bound ρ. The residual is given by $r = Qx - b$ with Q the involved operator and b the involved rhs.

Analytically comparing the bounds of the residual of the iterated solution of Eq. (3.3) and Eq. (3.4) one would be in favor of case **B** for $\mu < 1$. Indeed following Appendix A for the residuals we obtain

$$\frac{\|r_B\|}{\|b\|} \leq \left(1 + \sqrt{\frac{\lambda_{\max}^2 + \mu^2}{\lambda_{\min}^2 + \mu^2}} \right) \rho \qquad \text{and} \qquad \frac{\|r_C\|}{\|b\|} \leq \frac{\rho \sqrt{\lambda_{\max}^2 + \mu^2}}{|\mu|} , \tag{3.5}$$

where each inversion is stopped when the relative residual fulfills $r/b < \rho$. However, comparing the error

$$\frac{\|e_B\|}{\|b\|} \leq \frac{\rho}{\lambda_{\min}^2 + \mu^2} \qquad \text{and} \qquad \frac{\|e_C\|}{\|b\|} \leq \frac{\rho}{|\mu| \sqrt{\lambda_{\min}^2 + \mu^2}}. \tag{3.6}$$

it follows the error e_B of case B is numerical equivalent to the error e_C of case C if $\lambda_{min} \ll \mu$.

In the case of TM Wilson fermions at maximal twist this relation is fulfilled since $\lambda_{min} \sim 0$. This is the case in our example, shown in Fig. 3. CG solver and the two aforementioned multigrid approaches are analyzed using a stopping criteria of $\|r\| / \|b\| < 10^{-9}$ for our physical test ensemble. For this ensemble, $\lambda_{min}^2 + \mu^2 \simeq 0.00072^2$, thus yielding a difference around six orders of magnitude between residual and error, as shown in Fig. 3.

Despite the fact that as long as $\mu \gg \lambda_{min}$ all approaches yield a similar error, the approach **C** has advantages. The first advantage is that the software optimization is straightforward because both shifts can be solved together, as outlined in Ref. [22, 23]. The second advantage is that for the shifted linear equations it gives a better way to start the iteration with an optimal initial guess. Therefore, we consider this approach in what follows.

3.2 DD-αAMG for the non-degenerated twisted mass operator

The idea behind adapting the DD-αAMG approach to the ND twisted mass operator $D_{\mathrm{ND}}(\bar{\mu}, \bar{\epsilon})$ is based on preserving the $(\Gamma_5 \otimes \tau_1)$-symmetry on the coarse grid. We define the ND coarse grid operator by

$$D_{\mathrm{ND},c}(\bar{\mu}, \bar{\epsilon}) = P_{\mathrm{ND}}^\dagger D_{\mathrm{ND}}(\bar{\mu}, \bar{\epsilon}) P_{\mathrm{ND}}. \tag{3.7}$$

with P_{ND} being a suitable prolongation operator. If P_{ND} is $(\Gamma_5 \otimes \tau_1)$-compatible, i.e.

$$(\Gamma_5 \otimes \tau_1) P_{\mathrm{ND}} = P_{\mathrm{ND}} (\Gamma_{5,c} \otimes \tau_1), \tag{3.8}$$

it follows that the $(\Gamma_5 \otimes \tau_1)$-hermiticity of D_{ND} in Eq. (2.7) is also preserved on the coarse grid and the coarse grid operator fulfills

$$(\Gamma_{5,c} \otimes \tau_1) D_{\mathrm{ND},c} = P_{\mathrm{ND}}^\dagger (\Gamma_5 \otimes \tau_1) D_{\mathrm{ND}} P_{\mathrm{ND}} = P_{\mathrm{ND}}^\dagger D_{\mathrm{ND}}^\dagger (\Gamma_5 \otimes \tau_1) P_{\mathrm{ND}} = D_{\mathrm{ND},c}^\dagger (\Gamma_{5,c} \otimes \tau_1) . \tag{3.9}$$
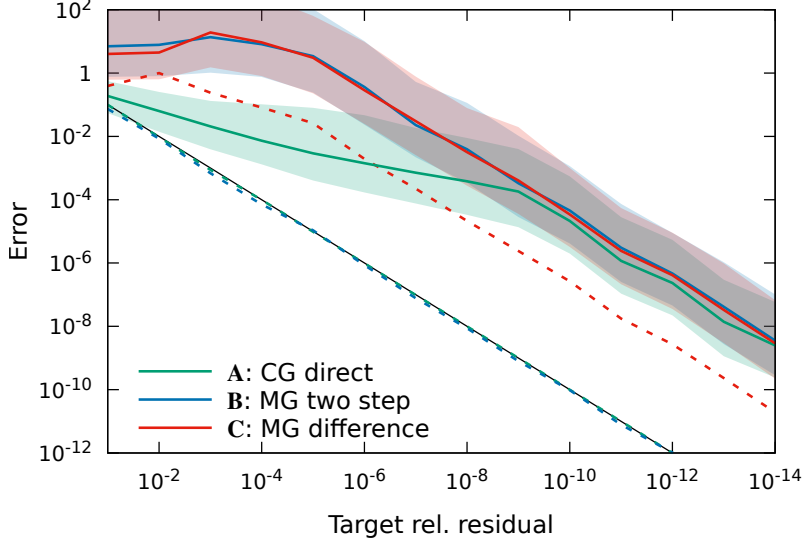
Figure 3: The dependence of the error and the residual on the stopping criterium for the three different ways of solving Eq. (3.2). Method **A** uses the conjugated gradient solver (green), method **B** uses the consecutively ordered single inversions of Eq. (3.3) (blue) and method **C** uses the single inversions involving differences (red) given by Eq. (3.4). The residuals are shown as dashed lines while the error is illustrated by the solid line with a shaded band determined by the largest and smallest local deviations as defined in Appendix A.

The property in Eq. (3.8) is satisfied by a prolongation operator P_{ND}, which is Γ_5-compatible and diagonal in flavor space. We choose identical components in flavor space defining $P_{\mathrm{ND}} = P \otimes I_2$. Thus, we obtain

$$D_{\mathrm{ND},c}(\bar{\mu}, \bar{\epsilon}) = (D_{\mathrm{W},c} \otimes I_2) + i\bar{\mu} (\Gamma_{5,c} \otimes \tau_3) - \bar{\epsilon} (I_c \otimes \tau_1) = \begin{bmatrix} D_{\mathrm{TM},c}(\bar{\mu}) & -\bar{\epsilon} I_c \\ -\bar{\epsilon} I_c & D_{\mathrm{TM},c}(-\bar{\mu}), \end{bmatrix} \quad (3.10)$$

which follows from the property $P^\dagger P = I_c$. We note that the flavor and spin components of the coarse operator preserve a similar sparse structure and properties of the fine grid operator $D_{\mathrm{ND}}(\bar{\mu}, \bar{\epsilon})$ in Eq. (2.1).

It follows from Eq. (3.1), that the prolongation operator P has to project onto a subspace, which captures the IR-modes. While P_{ND} is degenerate in flavor space, the low modes of the ND twisted mass operator are defined in the full space. Thus our solution to Eq. (3.8) i.e. $P_{\mathrm{ND}} = P \otimes I_2$ could spoil the efficiency of the coarse grid correction since the same prolongation operator P has to act on both flavor spaces. A possible solution is to use the prolongation operator P employed for the TM Wilson operator [16]. This has the advantage that if the multigrid solver is used during the HMC the same setup, built up for one flavor of the TM Wilson operator, can be reused in any step of the HMC for both light degenerate and heavy non-degenerate sector. Saving additional setup expenses makes the usage of the multigrid in HMC more effective. We will motivate this choice in section 3.2.1, and discuss some numerical results in section 3.2.2.

3.2.1 Motivations for the multigrid construction

The choice of the subspace $P_{\mathrm{ND}} = P \otimes I_2$ for Eq. (3.10) is motivated as follows:
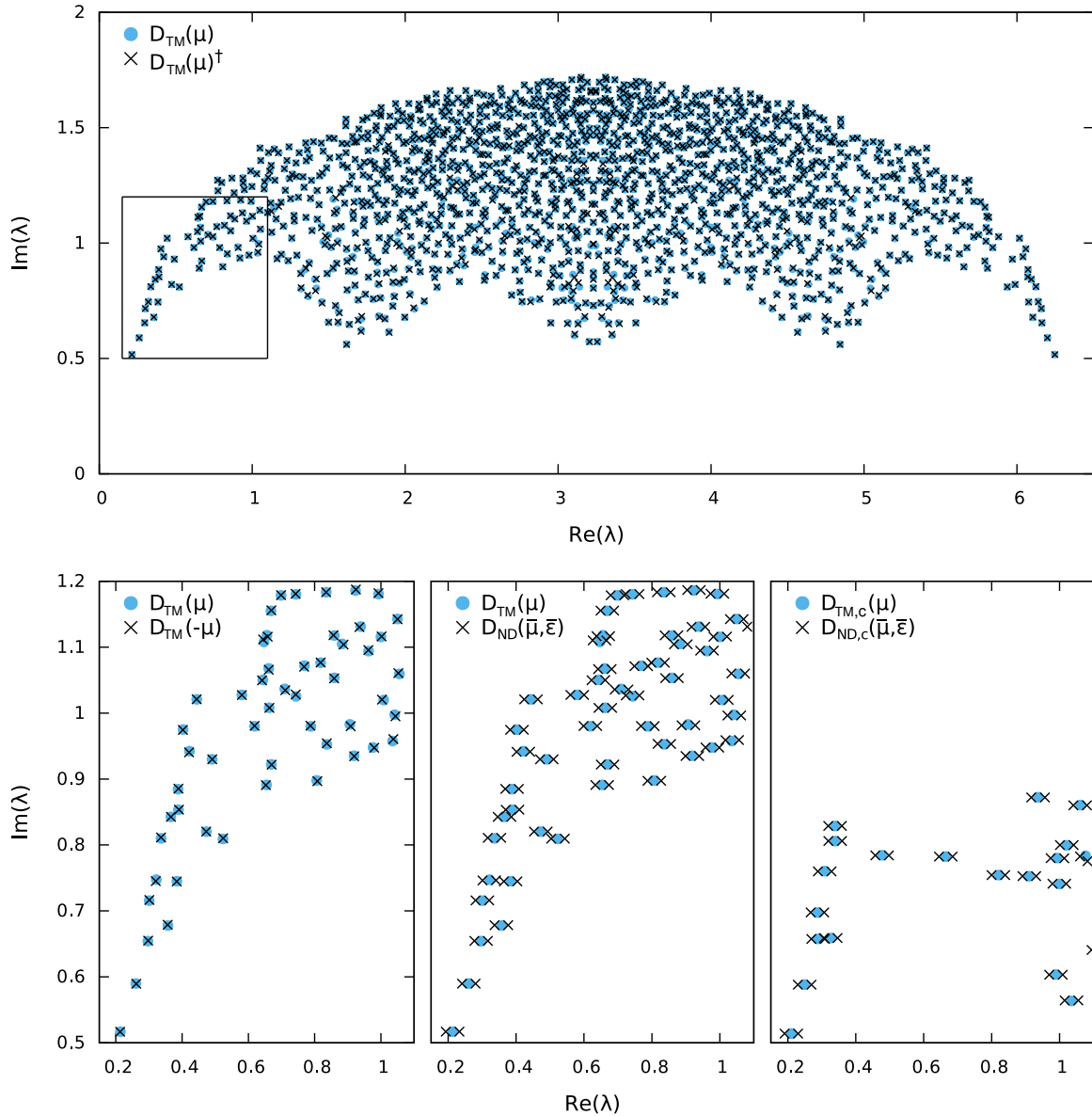
Figure 4: Complete spectrum of a gauge configuration for a lattice of size 4^4. The twisted mass parameters are $\mu, \bar{\mu}, \bar{\epsilon} = 0.01$. In the top panel, we depict the spectrum of the degenerate $D_{\mathrm{TM}}(\mu)$ operator folded with respect to the imaginary axis. In the bottom left panel we show part of the spectrum close to the origin for $D_{\mathrm{TM}}(\mu)$ for different sign of $\pm\mu$. In the central lower panel we compare the degenerate and non-degenerate TM operator. In the right lower panel, we show the spectrum for the coarse version of both operators.

- Let us consider first the case with $\bar{\epsilon} = 0$, for which the subspace needs to be effective for the TM Wilson operator $D_{\text{TM}}(\pm\mu)$ where μ can take both sign. This was analyzed numerically in Ref. [16,24] where it was found that the effectiveness of the subspace generated for the TM Wilson operator $D_{\text{TM}}(\mu)$ is affected only slightly if another parameter set is used with $D_{\text{TM}}(\pm\rho)$ where $\rho \geq \mu$.

  This can be explained by the connection between right-handed eigenvectors v_R of the TM Wilson operator $D_{\text{TM}}(\mu)$ and the left-handed eigenvectors $v_L = v_R^\dagger \Gamma_5$ of $D_{\text{TM}}(-\mu)$, which reads as

  $$D_{\text{TM}}(\mu)v_R = \lambda v_R \quad \Longleftrightarrow \quad v_R^\dagger \Gamma_5 D_{\text{TM}}(-\mu) = v_R^\dagger \Gamma_5 \lambda^\dagger. \tag{3.11}$$

  Thanks to the Γ_5 compatibility of the aggregation, this is also true for the coarse operator. Thus, the eigenspaces of $D_{\text{TM}}(\pm\mu)$ are connected and a prolongation operator P constructed for $D_{\text{TM}}(\mu)$ captures the low modes of $D_{\text{TM}}(\mu)$ when acting on the right while acting from the left givens the low modes of $D_{\text{TM}}(-\mu)$.

- Considering the case $D_{\text{ND}}(0, \bar{\epsilon})$ where $\bar{\mu} = 0$ and $\bar{\epsilon} \neq 0$, it follows that the eigenvalues have a linear dependency in $\bar{\epsilon}$ and the eigenvectors are degenerate in flavor space. Indeed the relation $D_{\text{ND}}(0, \bar{\epsilon})w_\pm = (\lambda \pm \bar{\epsilon})w_\pm$ with $w_\pm = (v, \pm v)$ holds in flavor space with the eigenvector v of D_W satisfying $D_\text{W}v = \lambda v$. Thus, for $\bar{\mu} = 0$ the eigenspace is invariant under changing $\bar{\epsilon}$ and it motivates the choice via Eq. (3.8) for the coarse grid projector.

- It follows that the choice for the projector of Eq. (3.8) is well-motivated for the special cases $\bar{\mu} \neq 0 \land \bar{\epsilon} = 0$ and $\bar{\mu} = 0 \land \bar{\epsilon} \neq 0$. However, what we have in reality is $\bar{\mu} \sim 0.1 \land \bar{\epsilon} \sim 0.1$. In order to verify if the properties mentioned in the previous two items are a good approximation, we study numerically the eigenvalue spectrum when changing the parameters $\bar{\mu}$ and $\bar{\epsilon}$ on a small lattice of a size of 4^4. The eigenvalue spectrum with positive imaginary part of the ND twisted mass operator is depicted in Fig. 4. Note that due to the $(\Gamma_5 \otimes \tau_1)$-hermiticity the real-axis is a symmetry axis, thus eigenvalues come in complex conjugated pairs or are real. For the one flavor operator $D_{\text{TM}}(\mu)$ this symmetry is broken for $\mu \neq 0$. This is shown in the left lower panel, where we focus on the spectrum of the low modes. By taking a closer look to the spectrum of the ND twisted mass operator, the real-axis symmetry is restored. Moreover, the parameter $\bar{\epsilon}$ for the non-degenerate operator $D_{\text{ND}}(\bar{\mu}, \bar{\epsilon})$ acts on the eigenvalues via a linear shift $\pm\bar{\epsilon}$ similar to the ideal case given by $D_{\text{ND}}(0, \bar{\epsilon})$. Thus, the projector given by Eq. (3.8) should project on the small eigenvalues of $D_{\text{ND}}(\bar{\mu}, \bar{\epsilon})$. For our case study, this is indeed the case as depicted in the right panel of Fig. 4. The spectrum of the coarse grid operator for the TM Wilson and ND twisted mass operator display similar features showing that preserving the operator structure in the coarse grid allows to preserve properties of the fine operator.

3.2.2 Numerical results

In this section we test the effectiveness of our choice $P_{\text{ND}} = P \otimes I_2$ using the physical test ensemble. We compare the performance of the multigrid solver using method **C**, see Eq. (3.4), to the one of the conjugate gradient solver in the case of the squared ND twisted mass operator at physical heavy quark parameters and additional at physical light quark parameters. Solving
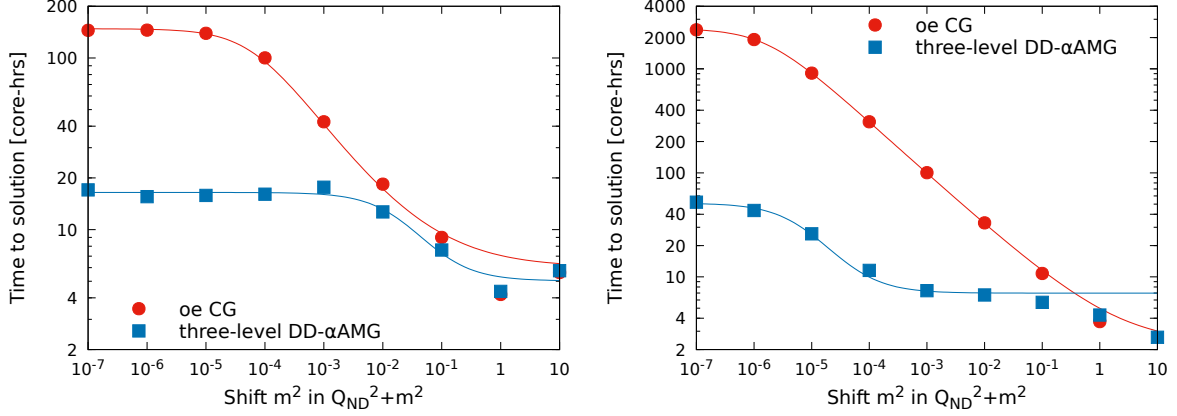
Figure 5: Comparison between time to solution for computing the inverse of the squared ND twisted mass operator at different shift m^2 using the odd-even (oe) CG solver and the DD-αAMG approach. We used the physical test ensemble employing physical strange and charm quark masses (left panel) and physical up and down quark masses (right panel).

the equation

$$x = (Q_{\mathrm{ND}}^2(\bar{\mu}, \bar{\epsilon}) + m^2)^{-1} b = \frac{i}{2m} (Q_{\mathrm{ND}}(\bar{\mu}, \bar{\epsilon}) + im)^{-1} b - (Q_{\mathrm{ND}}(\bar{\mu}, \bar{\epsilon}) - im)^{-1} b) \qquad (3.12)$$

for several shifts in m^2 we obtain the results shown in Fig. 5. The time to solution for the CG solver can be fitted by [25]

$$t_{CG}(m^2) = a + \frac{b}{\ln\left(1 - 2/(\sqrt{\kappa(m^2)} + 1)\right)} \qquad (3.13)$$

with the condition number $\kappa = (\lambda_{max} + m^2)/(\lambda_{min} + m^2)$. In the case of the heavy quark parameters it follows $\lambda_{max} = 4.7$ and $\lambda_{min} = 0.000065$ and at minimal χ^2 the parameters are given by $a = 5.88(123)$ and $b = -1.06(3)$. The fit approach used for the time to solution of the multigrid solver is motivated by the convergence of the general minimal residual solver (GMRES) [26]. We employ the functional form given by

$$t_{MG}(m^2) = A + \frac{B}{\ln(1 - (C + m^2)/(4.7 + m^2))} \qquad (3.14)$$

where we use, instead of the condition number, a modified function dependence given by $(C + m^2)/(4.7 + m^2)$. Minimizing χ^2 for the heavy quark parameters yields $A = 5.0(7)$, $B = -0.059(26)$ and $C = 0.024(10)$. Note that this is only an effective fit approach, which describes the data well but could fail for different cases. At the physical strange and charm quark masses – i.e. $m^2 \to 0$ see left panel of Fig. 5 – we found an order of magnitude speed-up of the multigrid approach compared to the CG solver. Moreover, the ND multigrid solver is even more effective than the multigrid solver for the TM Wilson operator at physical strange quark mass. This can be seen by comparing the relative speed-up for strange quark mass of $m_q \sim 95$ MeV, shown in Fig. 2 for the TM Wilson operator. The relative speed-up for two application of the ND-multigrid solver is comparable with the speed-up of a single application in case of the
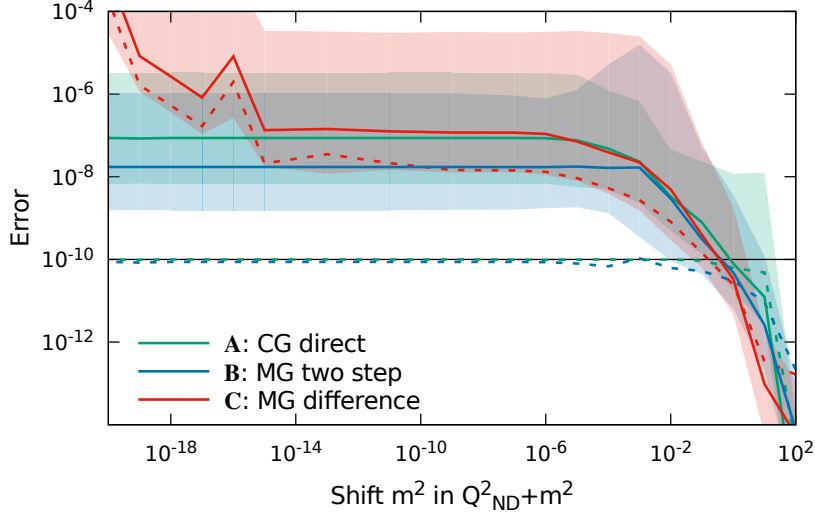
11

Figure 6: The dependence of the error and the residual on the shift m^2 for the three different approaches for solving the linear equation involving the ND twisted mass operator. Method A is given by the direct solution using the conjugate gradient solver (green), method B is given by the consecutively ordered single solves (blue) and method C is given by the difference of the two single solves (red). The residual are shown as dashed lines while the error is illustrated by the straight line attached to a shaded band given by the largest and smallest deviations as defined in Appendix A.

TM Wilson operator. This is also confirmed at physical non-degenerated light quark masses, as shown in the right panel of Fig. 5. Here we found a speed-up of around two orders of magnitude similar to the case of the TM Wilson operator. This shows that the choice of the coarse grid projector, building up using the TM Wilson operator, yields a very effective multigrid approach for the ND twisted mass operator.

Due to the large parameter set of multigrid approaches, optimization for a specific lattice can become a major task. In Ref. [16] we outlined our strategy and gave a set of parameters. We use this set of optimized parameters with a few adjustments in case of heavy quark masses. Namely, the shift d of the TM parameter in the coarse grid is set to unity and the number of smoothing iterations is reduced from 4 to 2.

As discussed in section 3.1, Eq. (3.12) with the squared operator can be solved in different ways. We analyze the connection of the error of the squared system with the residual of single systems for different shifts m at physical heavy ND parameters $\bar{\mu}$ and $\bar{\epsilon}$. The results are shown in Fig. 6. We fix the stopping criteria for each inversions to $\|r\| / \|b\| < 10^{-10}$. As discussed in section 3.1 and in Appendix A, they depend on the smallest eigenvalue of the operator $Q_{\mathrm{ND}}^2 + m^2$, which is given by $\lambda_{\mathrm{ND},min} \sim 0.0008$. As shown in Fig. 6 this bounds the error for the approach **A** and **B** by around 3 orders of magnitudes if $m < \lambda_{\mathrm{ND},min}$. For case **C** this is not true, however, numerically we find that the real error is similar to case **A** and **B** when $m^2 > 10^{-14}$. This shows that method **C** can be used for our application since in the rational approximation of the matrix square root all shifts are larger than $m^2 > 10^{-10}$.

4 Multigrid in rational approximation

In this section, we introduce a novel strategy for providing initial guesses to shifted linear systems as in Eq. (1.1) in order to optimize the usage of multigrid approaches in multi mass-shifted systems. We first give a brief introduction to the rational approximation of the square root of a hermitian matrix before we discuss how optimal initial guesses can be generated.

4.1 Rational approximation of the square root

Rational functions can be used to approximate analytical functions like the square root of a matrix, which is an essential ingredient for lattice QCD. For example, in case of the Rational Hybrid Monte Carlo (RHMC) [2], which is commonly used in the case of Wilson-type fermions for non-degenerate quark masses, staggered fermions and for calculating the sign-function needed for the Neuberger overlap operator. Here we are interested in solving

$$x = \sqrt{Q^{-2}}b \, . \tag{4.1}$$

In general a continuous function, like the square root, can be approximated by a rational function of generic order $[m, n]$

$$R(y) = A \frac{\prod_{i=1}^{m}(y + n_i)}{\prod_{i=1}^{n}(y + d_i)} \, . \tag{4.2}$$

The maximal deviation in a fixed interval of this rational approximation is then bounded from below, as stated in the de-Vallée-Poussin's theorem [27]. A rational approximation is optimal when the maximal deviation is equal to the bound. In case of the function $1/\sqrt{y}$ an optimal rational approximation is given by Zolotarev's solution [28]. The rational function of order $[n, n]$

$$R_{n,\epsilon}(y) = a_{n,\epsilon} \prod_{j=1}^{n} \frac{y + c_{n,\epsilon,(2j-1)}}{y + c_{n,\epsilon,2j}} \tag{4.3}$$

optimally approximates $1/\sqrt{y}$ in the interval $\epsilon < y < 1$ with a maximal deviation

$$\delta_{n,\epsilon} = \max_{\epsilon < y < 1} |1 - \sqrt{y} R_{n,\epsilon}(y)| \, . \tag{4.4}$$

The parameters in Eqs. (4.3,4.4) can be computed analytically [29] and they are given by

$$c_{n,\epsilon,k} = \mathrm{cs}^2 \left(k \cdot v_{n,\epsilon}, \sqrt{1 - \epsilon}\right) \qquad \text{with } v_{n,\epsilon} = \frac{K\left(\sqrt{1 - \epsilon}\right)}{2n + 1} \tag{4.5}$$

$$a_{n,\epsilon} = \frac{2}{1 + \sqrt{1 - d_{n,\epsilon}^2}} \prod_{j=1}^{n} \frac{s_{n,\epsilon,(2j-1)}}{s_{n,\epsilon,2j}} \qquad \text{with } s_{n,\epsilon,k} = \mathrm{sn}^2 \left(k \cdot v_{n,\epsilon}, \sqrt{1 - \epsilon}\right) \tag{4.6}$$

$$\delta_{n,\epsilon} = \frac{d_{n,\epsilon}^2}{1 + \sqrt{1 - d_{n,\epsilon}^2}} \qquad \text{with } d_{n,\epsilon} = (1 - \epsilon)^{\frac{2n+1}{2}} \prod_{j=1}^{n} s_{n,\epsilon,(2j-1)}^2 \tag{4.7}$$

where $\mathrm{sn}(u, k)$ and $\mathrm{cs}(u, k) = \mathrm{cn}(u, k)/\mathrm{sn}(u, k)$ are Jacobi elliptic functions and $K(k)$ is the complete elliptic integral.

The solution to the Eq. (4.1) with fixed ϵ and order n can be rewritten as a system with a sum over operators with multiple mass shifts given by

$$x \simeq R_{n,\epsilon}(Q^2)b = a_{n,\epsilon}\left(1 + \sum_{i=1}^{n} q_i \cdot (Q^2 + m_i^2)^{-1}\right)b \tag{4.8}$$

where

$$m_i^2 = c_{n,\epsilon,2i} \quad \text{and} \quad q_i = (c_{n,\epsilon,(2i-1)} - c_{n,\epsilon,2i})\prod_{j=1,j\neq i}^{n} \frac{c_{n,\epsilon,(2j-1)} - c_{n,\epsilon,2i}}{c_{n,\epsilon,2j} - c_{n,\epsilon,2i}} . \tag{4.9}$$

4.2 Initial guesses for shifted linear systems

Iterative solvers are initiated via a starting vector. In most of the cases, this vector is chosen to be zero, since it is the most safe starting point if the inverse is unknown. However, if parts of the inverse is known the iteration count can be minimized by starting with an initial vector close to the solution, e.g. this is done in the case of exact deflation where the smallest eigenvalues are used to preconditioning the system. Here, we discuss two approaches, proposing an initial guess based on previous solutions and via the MMS-CG solver.

4.2.1 Initial guesses via Lagrange interpolation

The idea for the case of multi-mass shifted systems is to use previously computed solutions, e.g. $x_1, \ldots, x_n$, to generate an initial guess for the next inversion of the solution x_{n+1}. This can be done by a polynomial interpolation of the previous solutions where the previous shifts enter as node points. A polynomial of degree $(n-1)$, which interpolates n solutions is then given by

$$p(m) = \sum_{i=1}^{n} l_{i,n}(m)x_i \quad \text{with } l_{i,n}(m) = \prod_{\substack{j=1 \\ j\neq i}}^{n} \frac{m - m_j}{m_i - m_j}, \tag{4.10}$$

where $l_{i,n}$ are the Lagrange polynomials. The initial guess for the $(n+1)$th system follows with $\tilde{x}_{n+1} = p(m_{n+1})$.

Let us compute the n solutions using the stopping criteria $\|r_i\|/\|b\| < \rho$, then an upper bound for the initial guess for the $(n+1)$th iteration is given by

$$\|\tilde{r}_{n+1}\| = \|b - (Q + m_{n+1}I)\tilde{x}_{n+1}\| \leq \rho\,\gamma_n\,\|b\| + \left\|\sum_{i=1}^{n} c_{i,n}(m_{n+1} - m_i)\,x_i\right\|, \tag{4.11}$$

where γ_n is the sum over the absolute values of the coefficients $c_{i,n} = l_{i,n}(m_{n+1})$. More details are given in Appendix B.

The second term of Eq. (4.11) can be approximated assuming $x_i = (Q + m_i)^{-1}b$ such that it can be cast into

$$\frac{\|\tilde{r}_{n+1}\|}{\|b\|} \lesssim \gamma_n\rho + \prod_{i=1}^{n} \frac{|m_{n+1} - m_i|}{\lambda_{\min} + m_i} \tag{4.12}$$

if $m_i > 0$ and Q a positive-(in)definite matrix with $\lambda_{\min} \geq 0$. The initial guess $\tilde{x}_{n+1}$ is bounded by two terms. The first term depends on the nodes m_i while the second term depends

additionally on the smallest eigenvalue of the matrix. It follows that $\|\tilde{r}_{n+1}\| / \|b\| > \rho$ since $\gamma_n > 1$. However, γ_n is known *at priori* such that the interpolation strategy can be adapted if γ_n becomes too larger. In our case the second term dominates the right hand side of Eq. (4.12) due to the dependence on λ_{min}. Moreover the second term is strictly smaller than one for the case $m_{n+1} < m_i$. This gives the optimal ordering to solve the multi-shifted problem via initial guesses with

$$m_1 > m_2 > \ldots > m_n > m_{n+1} > \ldots > m_N > 0, \tag{4.13}$$

whereby it follows

$$0 \leq \prod_{i=1}^{n} \frac{|m_{n+1} - m_i|}{\lambda_{\min} + m_i} < 1. \tag{4.14}$$

Finally, we remark that if the upper bound of Eq. (4.12) is smaller than 1, starting from $\tilde{x}_{n+1}$ will be always more efficient than from a zero vector.

4.2.2 Initial guesses via MMS-CG

Another possibility to guess a starting vector for the last $(N - n)$ shifts is given by using the MMS-CG solver. The general idea of the MMS-CG solver is to exploit the fact that the eigenspace of the shifted systems are identical. Thus the Krylov space generated for one of the shifts can be simultaneously used to iterate the other shifts.

If one generates the Krylov space for the most ill-conditioned system, here the Nth system, all other iteration vectors will converge to smaller residuals than the residual of the target system. However, if the system is too ill-conditioned, like it is in our case, the iteration count of the MMS-CG solver increases drastically and a hybrid-approach is potentially more efficient.

Our proposal is to solve the first n systems via the MMS-CG solver by generating the Krylov space for the nth system. This will generate the first n solutions $x_1, x_2, \ldots, x_n$. Furthermore, the MMS-CG solver can also predict guesses for the next m systems by iterating those together with the first n systems. Although the iteration vectors of these systems will not reach the target precision, at the iteration count where the nth system is converged, the iteration vectors will contain the full information of the generated Krylov space for the nth system. Based on this fact, for the $(n + 1)$th system, the MMS-CG solver generates an initial vector, which is in general closer to the target residual than using a Lagrange interpolation based on the n solutions.

4.3 Initial guesses for the rational approximation of the square root

In the following we will analyze the behavior of the initial guesses for the rational approximation of the square root in Eq. (4.8) for the ND twisted mass operator using the physical test ensemble at physical strange and charm quark masses. For that we choose a rational approximation consisting of 10 terms using the interval $(\epsilon_{\mathrm{ND}} ; 1]$ with $\epsilon_{\mathrm{ND}} = 0.000065/4.7$. Using Lagrange interpolation we obtain an upper bound for the initial guesses through Eq. (4.11), bounded by two terms, which depend on $\gamma_n(m)$ and the previous solutions x_i, respectively. The coefficient $\gamma_n(m)$ depends on the nodes of the interpolation given by the shifts m_i^2. Using an ordering $m_1 > m_2 > \ldots > m_N$ for the shifts we found for both cases that $\gamma_n(m_{n+1})$ is not larger than 2. This bounds the first term of Eq. (4.11) by 2ρ where ρ is the precision of the
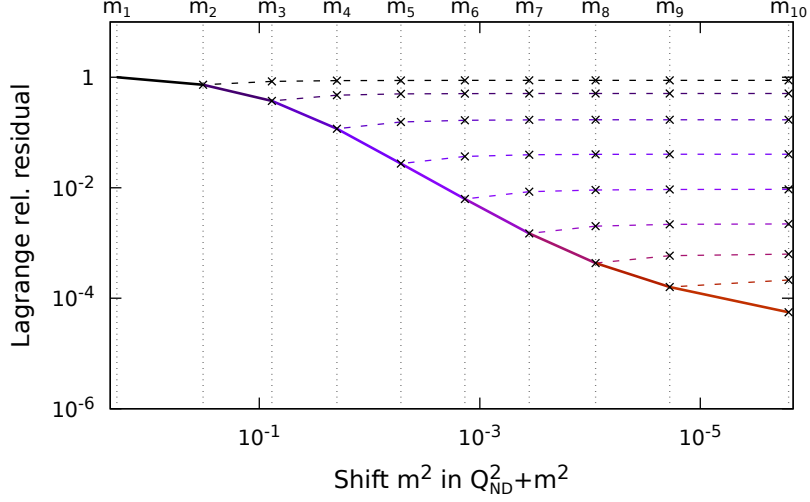
Figure 7: The relative residuals of the Lagrange interpolation based on the n solutions versus the shifts m^2 used in the approximation of the square root of the ND twisted mass operator. The solid lines illustrate the norm of the relative residual of the initial guess for decreasing m taking all available nodes into account. The nodes used in the interpolation, i.e. the shifts m^2, are denoted by vertical dotted lines. We depict the dependence of each polynomial $p^{(i)}$ for $m^2 > m_i^2$ by the dashed lines.

stopping criterion. Thus, the first term is suppressed compared to the second term of Eq. (4.11) such that we can neglect it in the following.

The second term of Eq. (4.11) can be approximated via

$$\left\| \sum_{i=1}^{n} c_{i,n}(m_{n+1} - m_i)\, x_i \right\| \simeq \prod_{i=1}^{n} \frac{|m_{n+1} - m_i|}{\lambda_{\min} + m_i} \tag{4.15}$$

with $\lambda_{\min} \sim 0.0008$ for the squared ND twisted mass operator. Using an ordering $m_1 > m_2 > \ldots > m_N$ this yields an upper bound of 0.0003 for the last, the Nth, initial guess, which is close to the residual shown in Fig. 7. However, for the first shifts the real residual is around one magnitudes lower than this bound. We find that the data can be described effectively via

$$\left\| \sum_{i=1}^{n} c_{i,n}(m_{n+1} - m_i)\, x_i \right\| \lesssim \prod_{i=1}^{n} \frac{|m_{n+1} - m_i|}{A_i m_i}, \tag{4.16}$$

where A_i is for all i smaller then 1.9. Using $B = [\max(A_i)]^{-1} < 1$ it follows

$$\left\| \sum_{i=1}^{n} c_{i,n}(m_{n+1} - m_i)\, x_i \right\| \simeq B^n \prod_{i=1}^{n} \left(1 - \frac{m_{n+1}}{m_i} \right) \tag{4.17}$$

with $m_{n+1} < m_i$ and $B \cong 0.6$. Thus, the initial guesses using the Lagrange interpolation become more efficient with increasing n, as shown in figure Fig. 7.

As pointed out in the previous section, the MMS-CG solver, used for solving the first n systems, can be used to predict an initial guess by including the $(N - n)$ systems in the MMS-CG iteration. This effectively interpolates the initial vector x_j in the Krylov space of the nth
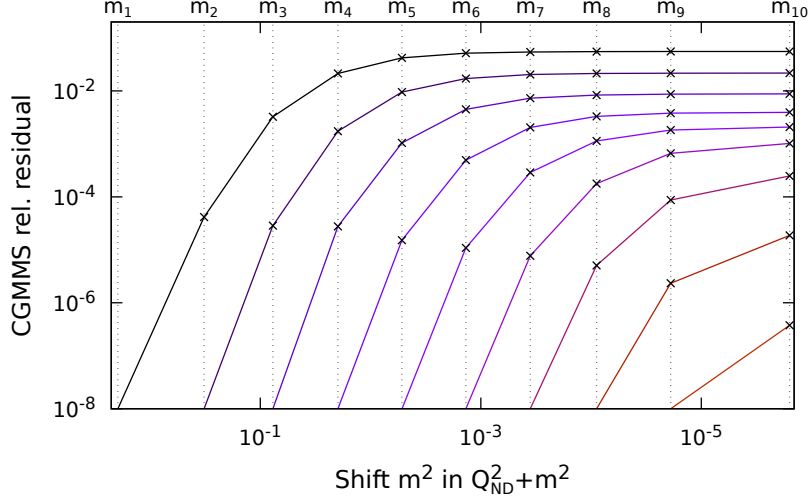
16

Figure 8: The relative residual of the iteration vectors of the MMS-CG versus the mass shifts when varying the target Krylov space for the ND twisted mass case. The solver is stopped when the residual of the target system reaches the stopping criterion given here by $\|r\| \, / \, \|b\| < 10^{-8}$. The iteration vectors of systems with smaller shift than the target one have a larger residual. This is shown for all $N-1$ cases depicted by the solid line changing the color from black, for the largest target shift to orange for the $N-1$ shift. Note that we do not show the case where the target system is given by the last, Nth system, because here all other systems have converged. The vertical dotted lines illustrate the shifts m_i^2.

system. We depict the residual for the predicted initial guesses by the MMS-CG solver in Fig. 8 if the nth system is converged. As shown, the relative residual of the $(n+1)$th system depends only slightly on n and is given by $\sim 10^{-5}$. Thus for the first step after using the MMS-CG solver the residual is smaller then the residual of the initial guess generated by the Lagrange interpolator. However, this changes for $m > 1$. While for small n the guess using the MMS-CG solver for the $(n+2)$th system is better, for $n \gtrsim 5$ the guesses of the Lagrange interpolation yield similar results and becomes better for $m > 2$.

Based on these results, the optimal approach for our example is a combination of all three elements, namely the MMS-CG solver and the Multigrid solver with initial guesses using the MMS-CG solver and the Lagrange interpolation. Thus, solving the first nth systems using MMS-CG solver involves an additional iteration for the $(n+1)$th and $(n+2)$th systems, which can be used as an initial guess. The $(N-n)$ remaining systems are then solved via a multigrid approach one by one where for the last $(N-n-2)$ systems the Lagrange interpolation is used to start the iteration. In the following section, we will discuss the optimal n.

4.4 Results

Based on the observations in the previous section, we propose to use a hybrid approach to solve a system of linear equations with N shifts. Namely, use the MMS-CG solver for the largest n shifts and the multigrid approach for the remaining $(N-n)$ systems solving each one via the difference methods discussed in section 3.1. The $(N-n)$ systems can be started by initial guesses, proposed for the $(n+1)$th and $(n+2)$th systems using the MMS-CG solver and for the rest using Lagrange interpolation and employing the previous solutions.
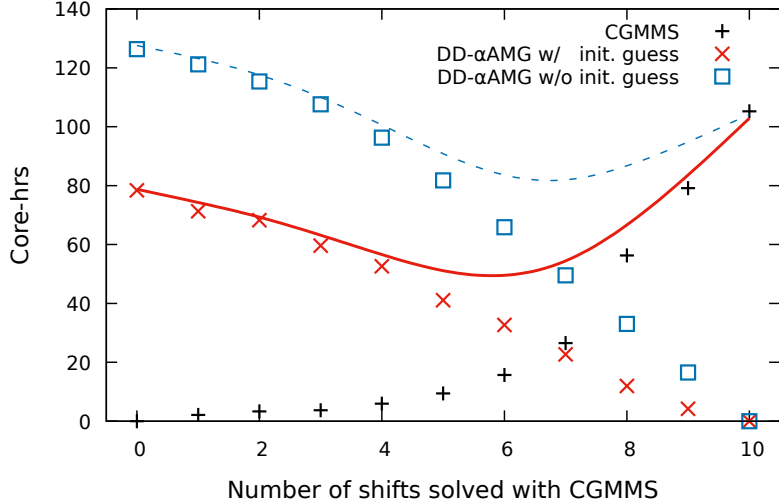
17

Figure 9: The CPU hours necessary to solve the multi-mass shifted equation involving the ND twisted mass operator at the strange and charm quark masses versus the number of shift n used in the MMS-CG solver shown as black crosses. The left $10 - n$ shifts are solved via the multigrid approach with initial guesses as red crosses and without initial guesses as blue squares. The total CPU hours needed to solve the system is shown by the red solid line for the hybrid method using initial guesses and for the hybrid method without initial guesses with the red solid line.

The optimal n depends on the ratio of the performance of the MMS-CG solver and the multigrid approach, which includes environmental parameters, software implementation and computer hardware. Here, we consider the Haswell-nodes partition of SuperMUC and use an MPI parallelization employing 1024 task on 37 nodes. The software used is the tmLQCD package [30, 31], which is linked to the DDalphaAMG library [32] and is publicly available.

The question we would like to answer is what is the optimal n of the hybrid approach introduce in this work, i.e. how many n shifts should be solved with the MMS-CG solver in order to solve the total system with N shifts in an efficient way employing for the last $N - n$ shifts a multigrid approach. This we discuss by employing the physical test ensemble using the ND twisted mass operator at the strange and charm quark masses with 10 mass-shifts. We employ case **C**, the difference method, for the linear equation with the squared operator when the multigrid solver is used.

The cost for the solution of the multi-mass shift linear equation via the hybrid method is given by

$$c_{HY}(n) = t_{CG}(m_n^2) + \sum_{i=n+1}^{N} t_{MG}(m_i^2) \, . \tag{4.18}$$

where the time to solution of the MMS-CG solver is approximated with the time of CG solver $t_{CG}(m)$ at the smallest shift m_n. For the case without initial guesses, the cost $c_{HY}(n)$ can be minimized using the fits Eqs. (3.13) and (3.14). This yields an optimal $n_{opt} \cong 7$ as shown in Fig. 9. However, the total speed-up of the hybrid method without initial guesses only improves slightly the time to solution compared to the application of the MMS-CG solver. This changes by using initial guesses. Here, the cost for the multigrid part is significantly reduced as shown in Fig. 9 using initial guesses compared to the case without. We find that the initial guesses reduce the total time to solution by about factor of two while the optimal $n_{opt} \sim 6$ is shifted
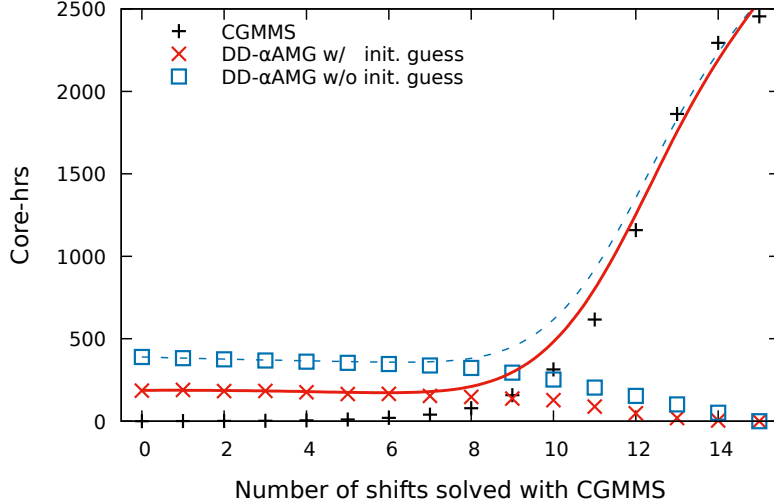
Figure 10: The CPU hours necessary to solve the multi-mass shifted equation involving the ND twisted mass operator for the physical value of the up and down quark mass. The dependence on the number of shift n used in the MMS-CG solver is shown as black crosses. The left $15 - n$ shifts are solved via the multigrid approach and results with initial guesses are shown with the red crosses while without initial guesses with the blue squares. The total CPU hours needed to solve the system is given by the red solid line for the hybrid method using initial guesses and with the dotted blue line for the hybrid method without initial guesses.

slightly.

The effect of this improvement can be also seen in the ensemble generation [20, 33], used in the HMC. When the force terms of the rational approximation are split to integrate shifts on different time scales, the time to solution of the heavy quark sector is reduced by a factor of approximately two. Note that the setup comes without additional cost due to the usage of the setup generated for the light quarks as discussed in section 3.2.

The hybrid method becomes even more effective for smaller quark masses. To illustrate this, the n-dependence is examined using the ND twisted mass operator at physical light quarks using the physical test ensemble. For $\bar{\mu}_\ell = 0.00072$ and $\bar{\epsilon}_\ell = 0.000348$ the dependence of the hybrid method using a rational approximation with $N = 15$ terms is shown in Fig. 10. We find that the hybrid method with initial guesses gives a total speed up at optimal $n_{opt} \cong 7$ by approximately a factor of 15. As in the case of the strange and charm quark masses, the initial guesses, result in a speedup of about a factor of two.

5   Conclusions

In this paper we examine multi-mass shifted system involving the ND twisted mass operator. We discuss in detail how the time to solution can be minimized using a hybrid method based on the MMS-CG solver in combination with a multigrid approach by using initial guesses. Using the heavy flavor doublet, and tuning to the physical values of the strange and charm quark masses, we find that employing a hybrid approach a speed up by a factor two can be achieved using for the six largest shifts the MMS-CG solver and for the smallest shifts the multigrid approach in combination with initial guesses. We show that for the light quark doublet this

hybrid approach yields even a larger improvement speeding up the time to solution by a factor of about 15.

The approach presented also speeds up the force calculation of the current $N_f = 2 + 1 + 1$ simulations of the ETM collaboration. Furthermore, this approach can be applied for all lattice fermion discretization for which a multigrid approach exists and a rational approximation is the choice to generated an ensemble of gauge configuration, e.g. like it is the case for the staggered discretization scheme.

One essential tool to speed up the hybrid method for the value of the strange quark mass is the usage of initial guesses. In this paper we show that a combination based on prediction via the MMS-CG solver and an approach based on Lagrange interpolation of the previous solutions yields the best time to solution.

We also discuss in detail the DD-αAMG approach, showing how to preserve symmetries of the fine grid operator on the coarse grid. Preserving the $(\Gamma_5 \otimes \tau_1)$-hermiticity of the ND twisted mass operator by employing a coarse grid projection based on the TM Wilson operator yields a stable multigrid method, yielding an overall speed-up of one magnitude compared to the CG solver at physical values of the strange and charm quark masses. This shows that the DD-αAMG approach is very effective as long as important symmetries are preserve on the coarse grid.

Furthermore, different ways for solving a linear equation with a shifted squared Dirac operator using iterative solvers are presented. While the CG solver can be used to solve this system directly the multigrid approach can be only applied to a system, which involves one Dirac operator. This results into two possible ways of solving the system, one using two consecutively solves and one using differences of single solutions. What has been shown in this work is that the latter can be used in the case of the ND twisted mass operator at physical strange and charm quark masses and yields some advantages if initial guesses are used.

Acknowledgments

References

[1] Roberto Frezzotti and Karl Jansen, *A Polynomial hybrid Monte Carlo algorithm*, Phys. Lett., **B402**, 328–334, 1997.

[2] M. A. Clark and A. D. Kennedy, *Accelerating dynamical fermion computations using the rational hybrid Monte Carlo (RHMC) algorithm with multiple pseudofermion fields*, Phys. Rev. Lett., **98**, 051601, 2007.

[3] Andreas Frommer, Stefan Güttel, and Marcel Schweitzer, *Efficient and stable Arnoldi restarts for matrix functions based on quadrature*, SIAM Journal on Matrix Analysis and Applications, **35**, no. 2, 661–683, 2014.

[4] Andreas Frommer, Stefan Güttel, and Marcel Schweitzer, *Convergence of restarted Krylov subspace methods for Stieltjes functions of matrices*, SIAM Journal on Matrix Analysis and Applications, **35**, no. 4, 1602–1624, 2014.

[5] Herbert Neuberger, *Exactly massless quarks on the lattice*, Phys. Lett., **B417**, 141–144, 1998.

[6] Beat Jegerlehner, *Krylov space solvers for shifted linear systems*, 1996.

[7] U. Glassner, S. Gusken, T. Lippert, G. Ritzenhofer, K. Schilling, and A. Frommer, *How to compute Green's functions for entire mass trajectories within Krylov solvers*, Int. J. Mod. Phys., **C7**, 635, 1996.

[8] Andreas Frommer and Uwe Glässner, *Restarted GMRES for Shifted Linear Systems*, SIAM Journal on Scientific Computing, **19**, no. 1, 15–26, 1998.

[9] M. Lüscher, *Local coherence and deflation of the low quark modes in lattice QCD*, JHEP, **07**, 081, 2007.

[10] R. Babich, J. Brannick, R. C. Brower, M. A. Clark, T. A. Manteuffel, S. F. McCormick, J. C. Osborn, and C. Rebbi, *Adaptive multigrid algorithm for the lattice Wilson-Dirac operator*, Phys. Rev. Lett., **105**, 201602, 2010.

[11] A. Frommer, K. Kahl, S. Krieg, B. Leder, and M. Rottmann, *Adaptive aggregation based domain decomposition multigrid for the lattice Wilson Dirac operator*, SIAM J. Sci. Comput., **36**, A1581–A1608, 2014.

[12] James Brannick, Andreas Frommer, Karsten Kahl, Björn Leder, Matthias Rottmann, and Artur Strebel, *Multigrid Preconditioning for the Overlap Operator in Lattice QCD*, Numer. Math., **132**, no. 3, 463–490, 2016.

[13] S. D. Cohen, R. C. Brower, M. A. Clark, and J. C. Osborn, *Multigrid algorithms for Domain-Wall fermions*, PoS, **LATTICE2011**, 030, 2011.

[14] Richard C. Brower, M. A. Clark, Alexei Strelchenko, and Evan Weinberg, *Multigrid for Staggered Lattice Fermions*, Submitted to: Phys. Rev. D, 2018.

[15] R. Frezzotti and G. C. Rossi, *Twisted mass lattice QCD with mass nondegenerate quarks*, Nucl. Phys. Proc. Suppl., **128**, 193–202, 2004, [,193(2003)].

[16] Constantia Alexandrou, Simone Bacchio, Jacob Finkenrath, Andreas Frommer, Karsten Kahl, and Matthias Rottmann, *Adaptive Aggregation-based Domain Decomposition Multigrid for Twisted Mass Fermions*, Phys. Rev., **D94**, no. 11, 114509, 2016.

[17] B. Sheikholeslami and R. Wohlert, *Improved Continuum Limit Lattice Action for QCD with Wilson Fermions*, Nucl. Phys., **B259**, 572, 1985.

[18] R. Frezzotti and G. C. Rossi, *Chirally improving Wilson fermions. 1. O(a) improvement*, JHEP, **08**, 007, 2004.

[19] R. Frezzotti and G. C. Rossi, *Chirally improving Wilson fermions. II. Four-quark operators*, JHEP, **10**, 070, 2004.

[20] C. Alexandrou et al., *Simulating twisted mass fermions at physical light, stange and charm quark masses*, in preparation, 2018.

[21] M. Lüscher, *Solution of the Dirac equation in lattice QCD using a domain decomposition method*, Comput. Phys. Commun., **156**, 209–220, 2004.

[22] Simon Heybrock, Matthias Rottmann, Peter Georg, and Tilo Wettig, *Adaptive algebraic multigrid on SIMD architectures*, PoS, **LATTICE2015**, 036, 2016.

[23] Daniel Richtmann, Simon Heybrock, and Tilo Wettig, *Multiple right-hand-side setup for the DD-αAMG*, PoS, **LATTICE2015**, 035, 2016.

[24] Simone Bacchio, Costantia Alexandrou, Jacob Finkenrath, Andreas Frommer, Karsten Kahl, and Matthias Rottmann, *DDalphaAMG for Twisted Mass Fermions*, PoS, **LATTICE2016**, 259, 2016.

[25] Yousef Saad, *Iterative methods for sparse linear systems*, vol. 82, siam, 2003.

[26] Jörg Liesen and Petr Tichý, *Convergence analysis of Krylov subspace methods*, GAMM-Mitt., **27**, no. 2, 153–173, 2004.

[27] Naum I Achieser, *Theory of approximation*, Courier Corporation, 2013.

[28] EI Zolotarev, *Application of elliptic functions to questions of functions deviating least and most from zero*, Zap. Imp. Akad. Nauk. St. Petersburg, **30**, no. 5, 1–59, 1877.

[29] Martin Lüscher, *Computational Strategies in Lattice QCD*, in: Modern perspectives in lattice QCD: Quantum field theory and high performance computing. Proceedings, International School, 93rd Session, Les Houches, France, August 3-28, 2009, pp. 331–399, 2010.

[30] K. Jansen and C. Urbach, *tmLQCD: A program suite to simulate Wilson twisted mass lattice QCD*, Comput. Phys. Commun., **180**, 2717–2738, 2009.

[31] S. Bacchio and J. Finkenrath, "tmLQCD interfaced to DDalphaAMG", Available at https://github.com/finkerath/tmLQCD.

[32] M. Rottmann, A. Strebel, S. Heybrock, S. Bacchio, and B. Leder, "DDalphaAMG", Available at https://github.com/DDalphaAMG/DDalphaAMG.

[33] Simone Bacchio, Constantia Alexandrou, and Jacob Finkenrath, *Multigrid accelerated simulations for Twisted Mass fermions*, in: 35th International Symposium on Lattice Field Theory (Lattice 2017) Granada, Spain, June 18-24, 2017, 2017.

[34] Martin Lüscher, *Stochastic locality and master-field simulations of very large lattices*, in: 35th International Symposium on Lattice Field Theory (Lattice 2017) Granada, Spain, June 18-24, 2017, 2017.

[35] Simon J Smith, *Lebesgue constants in polynomial interpolation*, in: Annales Mathematicae et Informaticae, vol. 33, pp. 1787–5021. Eszterházy Károly College, Institute of Mathematics and Computer Science, 2006.

A Error and residual of equivalent solutions

In this appendix we compare the numerical error and residual of solutions which are equivalent in exact arithmetic but not numerically. For clarity sake, our notation is the following: a linear system

$$Ax = b, \tag{A.1}$$

with A being an invertible matrix, b a known right hand side (rhs) and x the numerical solution, has residual and error, respectively,

$$r = b - Ax \quad \text{and} \quad e = A^{-1}b - x. \tag{A.2}$$

The residual is commonly used as stopping criterium for the solvers, since it does not require the knowledge of the *exact solution $A^{-1}b$*. However the error vector e is the statistical deviation which one introduces using the solution x. The error is connected to the residual by the relation

$$e = A^{-1}r \quad \text{which states} \quad \|e\| = \|A^{-1}r\| \leq \|A^{-1}\| \, \|r\| = \frac{\|r\|}{\sqrt{\lambda_{\min}(A^\dagger A)}}, \tag{A.3}$$

where the latter equality holds in the Euclidean norm and $\lambda_{\min}(A^\dagger A)$ is the smallest eigenvalue of $A^\dagger A$. Iterative solvers are usually stopped when $\|r\| < \rho \|b\|$ with ρ being a fixed tolerance. This fix the relative norm of the residual to be below a given threshold.

Hereafter we study and show numerical results for equivalent solutions in several cases. We use the TM Wilson operator on the physical test ensemble. In the numerical results we also show the error with maximal and minimal deviation of the local components. In the following examples we start from a random vector taken as the solution x. Then we apply the involved operator A to obtain the right hand side $b = Ax$. Then the error is given by $e = x' - x$ with x' the iterated solution. The minimal and maximal local deviation are given min/max of the norm of e restricted to the lattice site. The maximal and minimal deviation are potentially interesting for future simulations where very large lattices will be used [34]. Indeed since $\|b\|$ grows with $V^{1/2}$, the stopping criterium $\|r\| \leq \rho \|b\|$ does not guarantee the residual or error to be uniformly small and at larger V larger local deviation of the vectors are allowed.

A.1 Squared twisted mass operator

We start by taking a closer look to the linear system $(Q^2 + \mu^2 I)x = b$ which involves a squared hermitian operator Q^2. As already discussed in Section 3.1 we consider here the following three methods:

A: the linear system is directly solved by

$$x_A + e_A = (Q^2 + \mu^2 I)^{-1} b. \tag{A.4}$$

The solver stopping criterium is based on the relative residual of the solution, thus

$$\|r_A\| = \|b - (Q^2 + \mu^2 I) x_A\| \le \rho \|b\| \tag{A.5}$$

and norm of the error satisfies

$$\|e_A\| = \|(Q^2 + \mu^2 I)^{-1} r_A\| \le \frac{\|r_A\|}{\lambda_{\min}^2 + \mu^2} \le \frac{\rho \|b\|}{\lambda_{\min}^2 + \mu^2}. \tag{A.6}$$

B: the system is solved in two consecutive steps, by computing

$$x_\pm + e_\pm = (Q \pm i\mu I)^{-1} b \quad \text{and then} \quad x_B + e_B' = (Q \mp i\mu I)^{-1} x_\pm \tag{A.7}$$

using either x_+ or x_-. The solution

$$x_B + e_B = (Q^2 + \mu^2 I)^{-1} b \quad \text{has error} \quad e_B = e_B' + (Q \mp i\mu I)^{-1} e_\pm. \tag{A.8}$$

The solver stopping criteria are in the two steps respectively

$$\|r_\pm\| = \|b - (Q \pm i\mu I) x_\pm\| \le \rho \|b\| \tag{A.9}$$

$$\|r_B'\| = \|x_\pm - (Q \mp i\mu I) x_B\| \le \rho \|x_\pm\| \le \frac{\rho \|b\|}{\sqrt{\lambda_{\min}^2 + \mu^2}}. \tag{A.10}$$

The residual of the solution is then

$$r_B = b - (Q^2 + \mu^2 I) x_B = b - (Q \pm i\mu I)(x_\pm + r_B') = r_\pm + (Q \pm i\mu I) r_B'$$

$$\implies \|r_B\| < \|r_\pm\| + \|Q \pm i\mu I\| \|r_B'\| \le \left(1 + \sqrt{\frac{\lambda_{\max}^2 + \mu^2}{\lambda_{\min}^2 + \mu^2}}\right) \rho \|b\|. \tag{A.11}$$

For obtaining the smallest upper limit of the error in Eq. (A.8), we consider

$$e_\pm = (Q \pm i\mu I)^{-1} r_{\pm,B} \quad \implies \quad \|e_\pm\| \le \frac{\rho \|b\|}{\sqrt{\lambda_{\min}^2 + \mu^2}} \tag{A.12}$$

$$e_B' = (Q \mp i\mu I)^{-1} r_B' \quad \implies \quad \|e_B'\| \le \frac{\rho \|x_\pm\|}{\sqrt{\lambda_{\min}^2 + \mu^2}} \le \frac{\rho \|b\|}{\lambda_{\min}^2 + \mu^2} \tag{A.13}$$

from which we obtain

$$\|e_B\| = \|e_B' + (Q \mp i\mu I)^{-1} e_\pm\| \le \|e_B'\| + \frac{\|e_\pm\|}{\sqrt{\lambda_{\min}^2 + \mu^2}} \le \frac{2\rho \|b\|}{\lambda_{\min}^2 + \mu^2}. \tag{A.14}$$

C: the solution is given by a difference of two solutions of a linear combination of $x_\pm + e_\pm = (Q \pm i\mu)^{-1} b$,

$$x_C = b - (Q^2 + \mu^2) x_C = \frac{i}{2\mu}(x_+ - x_-) = (Q^2 + \mu^2 I)^{-1} b - \frac{i}{2\mu}(e_+ - e_-) \quad \text{for } \mu \ne 0. \tag{A.15}$$

The solver stopping criteria are in Eq. (A.9) and the errors $e_\pm$ in Eq. (A.12). The residual of the solution is then

$$r_C = \frac{i}{2\mu}\left((Q+i\mu I)r_+ - (Q-i\mu I)r_-\right)$$

$$\implies \|r_C\| \le \frac{1}{2\,|\mu|}\left(\|Q+i\mu I\|\,\|r_-\| + \|Q-i\mu I\|\,\|r_+\|\right) \le \frac{\rho\sqrt{\lambda_{\max}^2 + \mu^2}\,\|b\|}{|\mu|} \quad \text{(A.16)}$$

while the error of the solution is

$$e_C = \frac{i}{2\mu}(e_+ - e_-) \implies \|e_C\| \le \frac{1}{2\,|\mu|}(\|e_+\| + \|e_-\|) \le \frac{\rho\,\|b\|}{|\mu|\,\sqrt{\lambda_{\min}^2 + \mu^2}}. \quad \text{(A.17)}$$

Most of the numerical results are discuss in Section 3.1 and depicted in Fig. 3 for the $N_f = 2$ TM Wilson operator and in Fig. 6 for the ND twisted mass operator. Here we want to make some additional remarks which are the following ones:

- The error bounds of method **A**, **B** and **C** are compatible as long as the shift μ is larger than $\lambda_{\min}$. If the shift becomes smaller the error bound of method **C** increases inverse proportional. In our numerical example we found for all methods a comparable error, but only for the case $\mu < 10^{-14}$ with $\lambda_{\min} \sim 0.0008$ for the ND twisted mass case we found a deviation using method **C**. Here, methods **A** or **B** yield better results.

- The difference between the real error and the error bounds can give some information on the modes the solver tackles effectively. Namely if the real error coincidences with the error bound, the error is dominated by the mode of the smallest eigenvalue. In contrast, if the error is much smaller than the error bound, the error is dominated by much larger modes and thus the solver would treat the small eigenmodes very effectively. In our numerical test we found that in all cases the smallest eigenvalues are dominating the error. This is also the case if a multigrid solver is used. An explanation is that the coarse grid correction is calculated with a very large stopping criteria, which just tackle the low modes until the fine grid precision is reached.

- The error norm has a slope parallel to the target relative residual when the residual vector is dominated by a specific eigenvector. Indeed $\|e\| = \|(Q^2 + \mu^2 I)^{-1}r\| = \alpha\,\|r\|$ only if r is an eigenvector. In general the residual of standard Krylov solvers is dominated by the eigenvector with smallest eigenvalue which in this case is μ^2. This is indeed the separation we observe in Fig. 3 between error and relative target residual. Interestingly also multigrid methods produce solutions which have a residual dominated by the smallest eigenvalue. It is surprising because multigrid methods threat the low mode subspace separately and the convergence is expected to be similar for all the modes. For instance an exactly deflated solver would have the residual dominated by the first non-deflated eigenvalue. Moreover the multigrid residual is dominated by the smallest eigenvalue since target relative residual $\rho > 10^{-5}$ returning a solution with 100% error. This also explain why for inversions at high target relative residual, as in the molecular dynamics trajectory, we need with the DD-αAMG solver a more accurate solution than for the CG solver to satisfying the reversibility check at the same precision, as reported in Ref. [33].
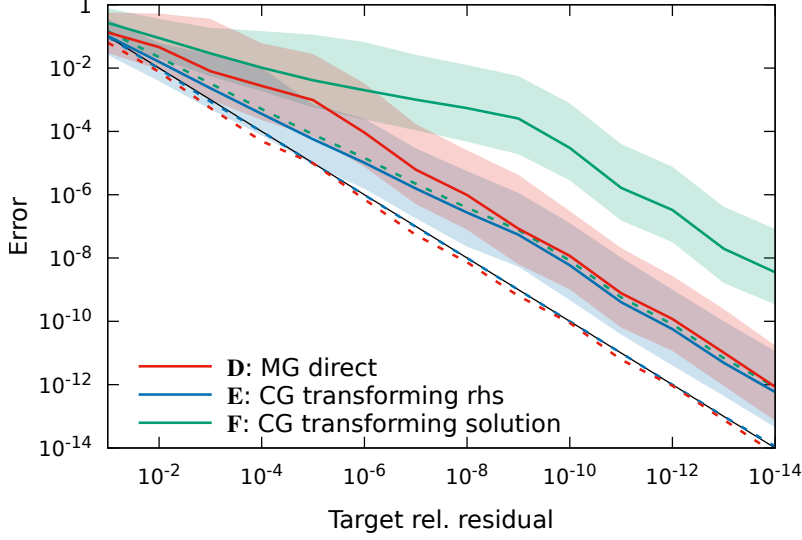
Figure 11: The dependence of the error and the residual on the stopping criteria for the three different approaches for solving the linear equation involving one single TM Wilson operator. Method **D** is given by the direct solution using the multigrid solver (red), method **E** is given by the CGNR method (blue) and method **F** is given by the CGNE method (green). The residual are shown as dotted lines while the error is illustrated by the straight line attached to a shaded band given by the largest and smallest deviations.

A.2 Single flavor twisted mass operator

In general retrieving the solution of the linear system in Eq. (A.1) can be done by different methods, for instance by using a linear iterative solver like the conjugate gradient (CG) solver. In case of CG, which requires A to be hermitian instead of Eq. (A.1) a modified linear equation involving a hermitian operator has to be solved. Two methods are available, known as CGNR and CGNE given by solving the equations

$$(A^\dagger A)x = A^\dagger b \quad \text{or} \quad (AA^\dagger)y = b \to x = A^\dagger y \tag{A.18}$$

for obtaining x respectively. Although both solutions are equivalent in exact arithmetic, in practice the numerical error and residual, as defined in Eq. (A.2), are in general different. In order to approach smaller quark masses and increasing the dimension of the lattice require to study different ways in order to control the resulting error.

Here we consider the following three methods for solving the linear equation $(Q \pm i\mu I)x_\pm = b$:

D: The linear system is solved directly by obtaining

$$x_{\pm,D} + e_{\pm,D} = (Q \pm i\mu I)^{-1}b. \tag{A.19}$$

The solver stopping criterium is based on the relative residual of the solution, thus

$$\|r_{\pm,D}\| = \|b - (Q \pm i\mu I)x_{\pm,D}\| \leq \rho \|b\|. \tag{A.20}$$

Following Eq. (A.3), the norm of the error satisfies

$$\|e_{\pm,D}\| = \left\|(Q \pm i\mu I)^{-1}r_{\pm,D}\right\| \leq \frac{\|r_{\pm,D}\|}{\sqrt{\lambda_{\min}^2 + \mu^2}} \leq \frac{\rho \|b\|}{\sqrt{\lambda_{\min}^2 + \mu^2}} \tag{A.21}$$

26

where $\lambda_{\min}^2$ is the smallest eigenvalue of Q^2.

E: A normal equation is used by applying a transformation on the rhs (equivalent to CGNR)

$$x_{\pm,E} + e_{\pm,E} = (Q^2 + \mu^2 I)^{-1}(Q \mp i\mu I)b. \tag{A.22}$$

Since the rhs is $(Q \mp i\mu I)b$, the solver stopping criterium is

$$\left\| r'_{\pm,E} \right\| = \left\| (Q \mp i\mu I)b - (Q^2 + \mu^2 I)x_{\pm,E} \right\| \le \rho \left\| (Q \mp i\mu I)b \right\| \le \rho \left\| b \right\| \sqrt{\lambda_{\max}^2 + \mu^2}. \tag{A.23}$$

The norm of the residual is then

$$\left\| r_{\pm,E} \right\| = \left\| (Q \mp i\mu I)^{-1} r'_{\pm,E} \right\| \le \frac{\rho \left\| (Q \mp i\mu I)b \right\|}{\sqrt{\lambda_{\min}^2 + \mu^2}} \le \rho \left\| b \right\| \sqrt{\frac{\lambda_{\max}^2 + \mu^2}{\lambda_{\min}^2 + \mu^2}} \tag{A.24}$$

and the norm of the error satisfies

$$\left\| e_{\pm,E} \right\| \le \frac{\left\| r_{\pm,E} \right\|}{\sqrt{\lambda_{\min}^2 + \mu^2}} \le \frac{\rho \left\| b \right\| \sqrt{\lambda_{\max}^2 + \mu^2}}{\lambda_{\min}^2 + \mu^2}. \tag{A.25}$$

F: A normal equation is used by applying a transformation on the solution (equivalent to CGNE)

$$y_F + e_F = (Q^2 + \mu^2 I)^{-1}b \quad \longrightarrow \quad x_{\pm,F} + e_{\pm,F} = (Q \mp i\mu I)y_F \tag{A.26}$$

where $e_{\pm,F} = (Q \mp i\mu I)e_F$. The solver stopping criterium

$$\left\| r_F \right\| = \left\| b - (Q^2 + \mu^2 I)y_F \right\| = \left\| b - (Q \pm \mu I)x_{\pm,F} \right\| = \left\| r_{\pm,F} \right\| \le \rho \left\| b \right\| \tag{A.27}$$

is equivalent to computing the residual of the solution $r_{\pm,F}$. The norm of the error then satisfies

$$\left\| e_{\pm,F} \right\| \le \frac{\left\| r_{\pm,F} \right\|}{\sqrt{\lambda_{\min}^2 + \mu^2}} \le \frac{\rho \left\| b \right\|}{\sqrt{\lambda_{\min}^2 + \mu^2}}. \tag{A.28}$$

From this analysis, we conclude that method **D** and **F** generates solutions which have compatible residuals and errors. On the other hand, method **E** has upper limits increased by the condition number $\kappa = \sqrt{(\lambda_{\max}^2 + \mu^2)/(\lambda_{\min}^2 + \mu^2)}$ compared to **D** or **F**. The numerical results depicted in Fig. 11 for the $N_f = 2$ twisted mass operator at the physical light quark mass ($\lambda_{\min}^2 = 0$ and $\mu = 0.00072$) confirm these conclusions. From the numerical results we also notice that the error of the method **E** is close to the upper limits obtained in Eq. (A.25). This shows that the residual of CG solver is dominated by the lowest eigenmodes. Indeed if $r = v_{\min}(A^\dagger A)$ holds, where $v_{\min}$ is the eigenvector of the smallest eigenvalue, then it follows

$$\| e \| = \left\| A^{-1}r \right\| = \left\| A^{-1} \right\| \| r \| = \frac{\| r \|}{\sqrt{\lambda_{\min}(A^\dagger A)}}. \tag{A.29}$$

B   Proof of concept for the initial guesses

As discussed in Section 4.2, we generate an initial guess for solving the $(n + 1)$th shifted linear system based on Lagrangian interpolation of the previous n solutions. The Lagrangian interpolation of a function $f(x)$ is given by

$$L_k(x) = \sum_{i=1}^{k} f(x_i) l_{i,k}(x) \tag{B.1}$$

where $k > 1$ and $l_{i,k}(x)$ satisfies $l_{i,k}(x_j) = \delta_{ij}$ for all $i, j \in [1, k]$ with δ_{ij} being the Kronecker delta. A polynomial solution to the latter property is

$$l_{i,k}(x) = \prod_{\substack{j=1 \\ j \neq i}}^{k} \frac{x - x_j}{x_i - x_j} \quad \Longrightarrow \quad l_{i,k}(x_j) = \delta_{ij} \text{ for } i, j \in [1, k] \tag{B.2}$$

where the Lagrangian interpolation defined via $l_{i,k}(x)$ is denoted as the Lagrange's form. In this case $L_k(x)$ is the unique polynomial of degree $(k-1)$ which exactly interpolates k fixed points of the function $f(x)$, i.e. $L(x_i) = f(x_i)$ for all $i \in [1, k]$. Additionally we define $l_{1,1}(x) \equiv 1$ which gives

$$\sum_{i=1}^{k} l_{i,k}(x) = 1 \qquad \text{for all } k \in \mathbb{N}^+ . \tag{B.3}$$

Furthermore it follows that the Lagrangian interpolation of a constant is exact, $L_k(x) = \sum_{i=1}^{k} b \, l_{i,k}(x) = b \sum_{i=1}^{k} l_{i,k}(x) \equiv b$. The Lagrangian interpolation of $(Q + mI)^{-1}$ with grid points $\{(Q + m_iI)^{-1}\}$ is given by

$$L_k(m) = \sum_{i=1}^{k} l_{i,k}(m)(Q + m_iI)^{-1} \quad \text{with } l_{i,k}(m) = \prod_{\substack{j=1 \\ j \neq i}}^{k} \frac{m - m_j}{m_i - m_j} . \tag{B.4}$$

The interpolated solution reads as

$$\tilde{x}_k(m) = L_k(m)b = \sum_{i=1}^{k} l_{i,k}(m)(Q + m_iI)^{-1}b = \sum_{i=1}^{k} l_{i,k}(m)x_i \tag{B.5}$$

where x_i are solutions of $(Q + m_iI)x_i = b$ computed with a residual $r_i = b - (Q + m_iI)x_i$ which fulfills the solver stopping criterium $\|r_i\| < \rho \|b\|$. For the residual of the interpolated solution $\tilde{x}_k(m)$ follows

$$\tilde{r}_k(m) = b - (Q + mI)\tilde{x}_k(m) = b - \sum_{i=1}^{k} l_{i,k}(m)(Q + mI)x_i \tag{B.6}$$

$$= \sum_{i=1}^{k} l_{i,k}(m) \left((m_i - m)x_i + b - (Q + m_iI)x_i \right) = \sum_{i=1}^{k} l_{i,k}(m) \left((m_i - m)x_i + r_i \right)$$

which is a Lagrangian interpolation of the residuals, i.e. $\tilde{r}_k(m_i) = r_i$. Studying the norm of the Lagrange's form of the residuals we obtain

$$\left\| \sum_{i=1}^{k} l_{i,k}(m) r_i \right\| \leq \sum_{i=1}^{k} |l_{i,k}(m)| \, \|r_i\| < \rho \, \|b\| \sum_{i=1}^{k} |l_{i,k}(m)| = \rho \, \gamma_k(m) \, \|b\| \tag{B.7}$$

where $\gamma_k(m) = \sum_{i=1}^{k} |l_{i,k}(m)|$ is the Lebesgue function defined from the Lagrange's polynomials $l_{i,k}(m)$. The Lebesgue function in the interval $[m_{\min}, m_{\max}]$ assumes values

$$1 \leq \gamma_k(m) \leq \Gamma_k \tag{B.8}$$

where $m_{\min}$ and $m_{\max}$ are the smallest and largest shifts of m_i, respectively, while $\Gamma_k = \max_{m \in [m_{\min}, m_{\max}]} \gamma_k(m)$ is referred to as Lebesgue constant. Depending on the shifts, the Lebesgue constant could grow as an exponential, logarithmic or asymptotic function of k [35]. In case of diverging growths one can truncate the degree of the interpolation in order to keep the error under control. The relation

$$\left\| \sum_{i=1}^{k} l_{i,k}(m) r_i \right\| \leq \rho \, \Gamma_k \, \|b\| \tag{B.9}$$

fixes the maximal contribution of the residuals to the residual of the interpolated solution.

The additional term to the Lagrange's form in Eq. (B.6) can be re-written as

$$\sum_{i=1}^{k} l_{i,k}(m)(m - m_i) x_i \simeq \left(\prod_{j=1}^{k} (m - m_j) \right) \sum_{i=1}^{k} \left(\prod_{\substack{j=1 \\ j \neq i}}^{k} \frac{1}{m_i - m_j} \right) (Q + m_i I)^{-1} b$$

$$= \left(\prod_{j=1}^{k} \frac{m - m_j}{Q + m_j I} \right) b \tag{B.10}$$

where $x_i \simeq (Q + m_i I)^{-1} b$ is used and the partial fraction decomposition is re-summed in a product of fractions. For the norm of follows

$$\left\| \sum_{i=1}^{k} l_{i,k}(m)(m - m_i) x_i \right\| \simeq \left\| \left(\prod_{i=1}^{k} \frac{m - m_i}{Q + m_i I} \right) b \right\| \leq \prod_{i=1}^{k} \frac{|m - m_i|}{|\lambda_{\min,i}|} \, \|b\| \tag{B.11}$$

where $\lambda_{\min,i}^2$ is the smallest eigenvalue of $(Q + m_i)^{\dagger}(Q + m_i)$. If Q is a positive-definite matrix then $\lambda_{\min,i} = \lambda_{\min} + m_i$ with $\lambda_{\min} > 0$ being the smallest eigenvalue of Q.

Considering now the full residual interpolation in Eq. (B.6) we find the following upper limits

$$\|\tilde{r}_k(m)\| = \left\| \sum_{i=1}^{k} l_{i,k}(m) \left((m - m_i) x_i + r_i \right) \right\| \leq \left\| \sum_{i=1}^{k} l_{i,k}(m)(m - m_i) x_i \right\| + \rho \, \gamma_k(m) \, \|b\|$$

$$\lesssim \left(\prod_{i=1}^{k} \frac{|m - m_i|}{|\lambda_{\min,i}|} + \rho \, \Gamma_k \right) \|b\| . \tag{B.12}$$

The first upper bound requires a knowledge of the solutions x_i and residuals r_i, making it dependent on the numerical approach. The second instead depends only on the analytical properties of the shifted systems.